



Get Clarity On Generics

Cost-Effective CT & MRI Contrast Agents

**FRESENIUS
KABI**

WATCH VIDEO

AJNR

This information is current as
of August 3, 2025.

**Comparing the Double-Echo Steady State
with Water Excitation and Constructive
Interference in Steady State Sequence
Techniques for Identifying Extracranial
Facial Nerve and Tumor Positions in Patients
with Parotid Tumors**

Xiaoxue Fan, Changwei Ding, Guyue Zhao and Yang Hou

AJNR Am J Neuroradiol published online 18 April 2024
<http://www.ajnr.org/content/early/2024/08/01/ajnr.A8309>

Comparing the Double-Echo Steady State with Water Excitation and Constructive Interference in Steady State Sequence Techniques for Identifying Extracranial Facial Nerve and Tumor Positions in Patients with Parotid Tumors

 Xiaoxue Fan,  Changwei Ding,  Guyue Zhao, and  Yang Hou



ABSTRACT

BACKGROUND AND PURPOSE: Reliable preoperative visualization of facial nerve morphology and understanding the spatial relationship between the facial nerve and tumors in the parotid gland can help clinicians perform safe and effective surgeries. Hence, this study aimed to compare the image quality of extracranial facial nerves obtained by using double-echo steady state with water excitation (DESS-WE) and CISS sequences and evaluate their diagnostic efficacy in the localization of parotid tumors.

MATERIALS AND METHODS: In total, 32 facial nerves of 16 healthy volunteers and 25 facial nerves of 25 patients with parotid tumors were included in this retrospective study. All participants underwent noncontrast-enhanced extracranial facial nerve MR imaging with DESS-WE and CISS with a 3T MR scanner equipped with a 64-channel head and neck coil. Image quality was subjectively evaluated by using a 5-point Likert scale by 2 radiologists. Inter- and intrarater agreements were assessed by using the Cohen κ coefficient. Receiver operating characteristic analysis was performed, and the diagnostic efficacies of DESS-WE and CISS images in localizing parotid tumors were calculated.

RESULTS: For healthy volunteers (11 men and 5 women; median age, 26 years), image quality scores for CISS were significantly higher than those for DESS-WE for the discrimination of the temporofacial and cervicofacial trunks (both, $P < .001$). In patients with parotid tumors (12 men and 13 women; median age, 58 years), CISS performed better than DESS-WE in terms of visualizing the spatial relationship of the facial nerve to the tumor and diagnostic confidence (both, $P < .001$). Regarding the localization of parotid tumors, CISS showed excellent performance, comparable to that of DESS-WE (area under the curve, 0.981 versus 0.942, $P = .1489$).

CONCLUSIONS: CISS achieved diagnostic performance comparable to DESS-WE in parotid tumor localization, with favorable image quality and more reliable morphologic visualization of the facial nerve.

ABBREVIATIONS: CNR = contrast-to-noise ratio; DESS-WE = double-echo steady state with water excitation; IQS = image quality score; IQR = interquartile range

The standard treatment for parotid tumors is surgical resection, and facial nerve injury is one of the most serious complications associated with parotid surgery.¹⁻³ However, when the facial nerve is distorted and displaced owing to tumor compression, visual identification, which is usually reliable for facial nerves, becomes difficult.^{4,5} Even with intraoperative facial nerve monitoring, 2%–6% of patients develop permanent facial palsy after parotidectomy,⁵⁻¹⁰ which severely affects their quality of life. Therefore, complete resection while preserving facial nerve

function is the main goal of parotid tumor surgery.^{2,11} Notably, facial palsy is related to the location of the parotid tumor, more than 35% of patients with deep-lobe tumors have been reported to develop temporary facial nerve palsy postoperatively,¹² and the rate of postoperative facial palsy is higher in patients with lesions involving the deep lobes than in those without.^{2,4,10,11} Surgery for deep-lobe tumors of the parotid gland may require extensive circumferentially dissected peripheral nerve dissections; the increased extent of the facial nerve dissection may contribute to temporary facial nerve palsy, leading to a higher incidence of permanent facial nerve palsy and consequently increasing the technical difficulty.¹³ Therefore, accurate preoperative localization of the tumor and thoroughly explaining the potential risk of postoperative facial nerve palsy to patients are important clinical issues.

MR tractography has been used by head and neck specialists as a reliable and valid tool for identifying facial nerves. This

Received December 23, 2023; accepted after revision April 8, 2024.

From the Department of Radiology, Shengjing Hospital of China Medical University, Shenyang, China.

Please address correspondence to Yang Hou, Department of Radiology, Shengjing Hospital of China Medical University, Shenyang 110004, China; e-mail: houyang1973@163.com



Indicates article with online supplemental data.

<http://dx.doi.org/10.3174/ajnr.A8309>

SUMMARY

PREVIOUS LITERATURE: DESS-WE images show the facial nerve trunk well in both healthy patients and patients with parotid tumors and have high diagnostic accuracy for the localization of parotid tumors.

KEY FINDINGS: CISS images can be used for preoperative visualization of the extracranial facial nerve. CISS images provide reliable imaging of the location of the facial nerve relative to the lesion in patients with parotid tumors.

KNOWLEDGE ADVANCEMENT: CISS demonstrates better visualization of the facial nerve branches (temporofacial and cervicofacial trunks) compared with DESS-WE. Moreover, CISS is a reliable method for identifying the locations of parotid tumors.

technique can produce high-contrast anatomic atlases and is particularly reliable for identifying facial nerve contact points with parotid tumors.^{14,15} However, it is not ideal for visualizing uncompressed branches of facial nerves.¹⁶ The reliable preoperative visualization of facial nerve morphology and understanding the spatial relationship between the facial nerve and tumor in the parotid gland can help clinicians perform safer and more effective surgeries.¹⁷ Early preoperative identification of the course of the facial nerve provides more reliable images of the facial nerve and helps surgeons to safely and effectively resect tumors, avoid potentially harmful manipulations, and reduce mechanical trauma. Nonetheless, the reliable and direct observation of the extracranial segment of the facial nerve remains challenging.

High-resolution MR techniques, including a 3D double-echo steady state with water excitation (DESS-WE) sequence, have been attempted for direct visualization of the extracranial segment of the facial nerve and have been reported to have excellent performance.^{18–20} The DESS-WE sequence reportedly can reliably depict morphology of the extracranial segment of the facial nerve as well as the relationships to parotid tumors, with high diagnostic efficacy in terms of tumor localization^{19,21,22}; however, this technique has limited ability in terms of visualizing the branches of the facial nerve.¹⁹ The 3D CISS sequence, with its high resolution and clear visualization of small anatomic structures, has been widely used for the morphologic assessment of the facial and cochlear nerves in the internal auditory canal.²³ A study demonstrated that the CISS sequence can clearly show the temporofacial and cervicofacial branches of the facial nerve; however, the number of patients with parotid tumors with localizations that were confirmed by surgery in that study was small ($n = 3$).²⁴

Therefore, this study aimed to compare the quality of images obtained using DESS-WE and CISS sequences, compare their relative ability to show the extracranial segments of facial nerves, and evaluate their diagnostic efficacy in terms of the localization of parotid tumors.

MATERIALS AND METHODS

Ethics Statements

This retrospective study was approved by our hospital's institutional review board (No. 2023PS144J), and written informed consent was obtained from all participants.

Study Participants

From June 2022 to July 2023, volunteers and patients with parotid tumors were prospectively recruited. Healthy volunteers

included participants aged ≥ 18 years. The exclusion criteria for the healthy volunteers were as follows: 1) history of head and neck tumors, 2) history of mumps, 3) history of head and neck surgery, 4) history of smoking, and 5) claustrophobia precluding MR imaging.

Patients with parotid tumors comprised participants who met the following inclusion criteria: 1) having undergone routine preoperative MR examination of the parotid gland and sequences of the extracranial segment of the facial nerve (including DESS-WE and CISS), 2) having received subsequent surgical treatment, 3) having detailed records of the location of the parotid tumor, and 4) age ≥ 18 years. Patients whose MR imaging studies had an image quality deemed insufficient for diagnosis by radiologists were also excluded.

Imaging Acquisition

All examinations were performed using a Magnetom Prisma 3T MR scanner (Siemens) equipped with a 64-channel head and neck coil. The detailed MR image parameters of DESS-WE and CISS are provided in Table 1. Both DESS-WE and CISS sequence scans included the region from the stylomastoid foramen to the mandible; these 2 imaging sequences typically required approximately 20 minutes of acquisition time. In addition to the DESS-WE and CISS sequences, we obtained routine spin-echo parotid MR images, including T1-weighted, T2-weighted, and T2-weighted fat-suppression images.

Quantitative Image Analysis

The original images were sent to the IntelliSpace Portal (Phillips) workstation for quantitative image analysis. The ROIs used for the analysis in each region were drawn by 2 radiologists with 26 and 9 years of experience with parotid MR interpretation, respectively. The signal intensity of the extracranial segment of the main trunk of the facial nerve was measured by using an ovoid ROI of minimal size (1 mm^2). The short axis of the ellipse of the ROI should not exceed the extent of the facial nerve (Online Supplemental Data). An ROI of the same size and same shape was placed on parotid tissue on the same image section to measure its signal intensity, avoiding the area encompassing blood vessels. The ROI for the background noise measured in the air was also selected on the same image section of the same size and same shape as the facial nerve (Online Supplemental Data). The ROI placement was consistently in its anatomic location, shape, and size across both DESS-WE and CISS sequences. The above quantitative data were measured separately by the 2 radiologists

Table 1: Parameters for DESS-WE and CISS sequences

Parameter	DESS-WE	CISS
TR (ms)	13.64	5.83
TE (ms)	4.68	2.57
Section thickness	0.5	0.5
Field of view (mm)	160 × 160	160 × 160
Matrix size	320 × 320	320 × 320
Voxel size (mm)	0.5 × 0.5 × 0.5	0.5 × 0.5 × 0.5
Band width (Hz/pixel)	315	504
Flip angle (°)	28	45
Acceleration method	PAT (GRAPPA)	—
Number of acceleration factor	2	—
Gradient times	80 mT/m, 200 T/m/s	80 mT/m, 200 T/m/s
Number of averages	1	1
Fat suppression	Water excitation	—
Number of sections	160	160
Acquisition time	7 minutes, 39 seconds	10 minutes, 18 seconds

Note:—GRAPPA indicates generalized autocalibrating partially parallel acquisitions; PAT, parallel acquisition technique.

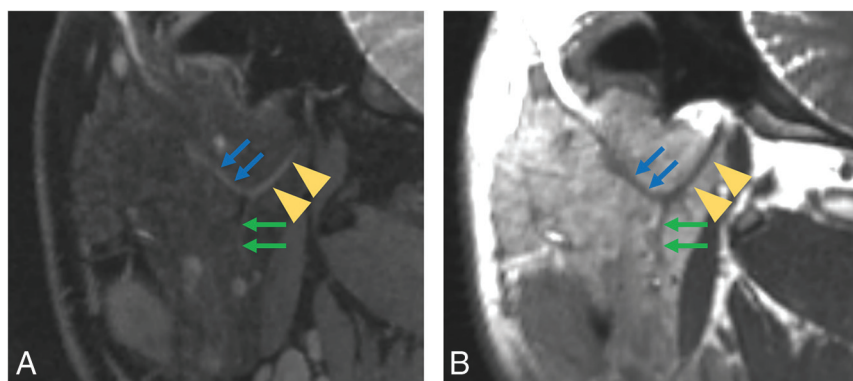


FIG 1. Standard observation slices for the image-based evaluation of the main, temporofacial, and cervicofacial trunks of the extracranial facial nerve of healthy volunteers in the oblique sagittal plane. The facial nerve shows a high signal on the DESS-WE image (A) and a low signal on the CISS image (B), with yellow arrowheads identifying the main trunk of the facial nerve, blue ones identifying the temporofacial trunk, and green ones pointing out the cervicofacial trunk.

and analyzed using mean values. SNR was first calculated as follows: $SNR_{fn} = \text{mean signal intensity of facial nerve} / \text{standard deviation of background noise}$; $SNR_{pp} = \text{mean signal intensity of parotid parenchyma} / \text{standard deviation of background noise}$.²⁵ Next, contrast-to-noise ratio (CNR) was calculated between the facial nerve (SNR_{fn}) and parotid parenchyma (SNR_{pp}) as follows: $CNR = SNR_{fn} - SNR_{pp}$.²⁶

Qualitative Image Analysis

All images were uploaded to our picture archiving and communication system workstation for subsequent evaluation. The 2 radiologists independently scored the image quality by using a 3D reconstruction postprocessing function. The facial nerve showed a high signal on DESS-WE images and a low signal on CISS images. DESS-WE and CISS images were scored using a 5-point Likert scale in healthy volunteers and patients with parotid tumors. The parotid facial nerve exits from the stylomastoid foramen and then divides into the temporofacial and cervicofacial divisions in the parotid gland.^{19,24} In healthy volunteers, the visibility of the main trunk of the extracranial segment of the facial nerve and the proximal temporofacial and cervicofacial divisions

were assessed on a reformatted sagittal oblique image that displays the main trunk and its bifurcation into the proximal temporofacial and cervicofacial divisions (Fig 1). In patients with parotid tumors, the clarity of tumor margin, the continuity of the facial nerve trunk from the foramen to the level of the parotid tumor, the spatial relationship between the facial nerve and the parotid tumor, and the diagnostic confidence level were each assessed on a scale of 1 to 5 (Online Supplemental Data). For each of these parameters, an image quality score (IQS) of ≥ 3 was considered satisfactory. The 2 radiologists reassessed the 2 sets of images for each patient again after at least 4 weeks to assess inter- and intrarater agreements and avoid recall bias.

Evaluation of the Efficacy of Parotid Tumor Localization

Parotid tumors were classified into 2 subgroups on the basis of Kim et al's criteria¹⁹: 1) deep lobe —, tumors not involving the deep lobe and located exclusively lateral to the facial nerve, and 2) deep lobe +, tumors involving the deep lobe, including those exclusively medial to the facial nerve, or that have components both medial and lateral to the facial nerve. Radiologists used the multiplanar postprocessing function to assess the spatial relationship between the extracranial facial

nerve and the parotid tumor on DESS-WE and CISS images for localization (Fig 2). For each lesion, the 2 radiologists made independent diagnoses, and both were blinded to the patient's surgical data or results. The diagnostic efficacy of DESS-WE and CISS images for determining whether a tumor is deep lobe — or deep lobe + was assessed by using the relative location of the facial nerve and the parotid tumor as seen during surgery, which is currently considered to be the reference standard.

Statistical Analysis

Nonnormally distributed variables are presented as medians. The Wilcoxon signed-rank test was used to compare the IQS of DESS-WE and CISS images. After testing the normality of continuous variables by using the Shapiro-Wilk test, normally distributed variables were represented by the mean value \pm standard deviation. Inter- and intrarater agreements for the IQS were evaluated by using the Cohen κ coefficient. The weighted κ coefficient was defined as follows: poor (0.00–0.20), fair (0.21–0.40), moderate (0.41–0.60), good (0.61–0.80), and excellent (0.81–1.00).^{27,28} If the 2 radiologists' subjective evaluation of the IQS showed good agreement (κ value > 0.60), the IQS of the more senior

radiologist was used as the final IQS for comparison to simplify scoring. The accuracy, sensitivity, and specificity of the DESS-WE and CISS image data were calculated, and the diagnostic efficacies of the 2 sets of images were compared by using receiver operating characteristic analysis. All data were analyzed by using SPSS software version 26.0 (IBM) and MedCalc Statistical Software version 19.6 (MedCalc Software). A *P* value of $<.05$ was considered statistically significant.

RESULTS

Patient Characteristics

In total, 16 healthy volunteers (11 men and 5 women; median age, 26 years; age range, 19–71 years) were enrolled. Hence, 32 facial nerves (2 per healthy volunteer) were imaged. Twenty-eight patients with parotid tumors met the inclusion criteria, of whom 3 were excluded: 2 because of severe swallowing artifact on MR

images and 1 because the facial nerve location could not be accurately confirmed surgically owing to the aspiration of cyst contents altering anatomic configuration of the tumor and regional structures. Hence, the final cohort comprised 25 patients (12 men and 13 women; median age, 58 years; range, 28–84 years) with a total of 30 parotid tumors: 3 ipsilateral Warthin tumors in 1 patient, 2 bilateral Warthin tumors in 2 patients, and 1 small cell carcinoma and 1 ipsilateral lymph node metastasis in 1 patient (Online Supplemental Data).

Quantitative Comparison of DESS-WE and CISS Images

The SNR_{in} was significantly lower in DESS-WE images than in CISS images ($P < .001$ for all; Table 2). In addition, regarding analysis of the obtained CNR, the CNR of the CISS image was significantly higher than that of the DESS-WE image in all analyzed participants (healthy volunteers and patients; $P < .001$ for all; Table 2).

Subjective Evaluation of DESS-WE and CISS Images in Healthy Volunteers

In the healthy volunteers, good inter- and intrarater agreements for IQS ($\kappa = 0.724$ – 0.816) were observed (Table 3). Both radiologists could distinguish the facial nerve trunk well on DESS-WE and CISS images; however, the IQS of facial nerve trunk visibility on CISS images (median: 5, interquartile range [IQR]: 4–5) was higher than that on DESS-WE images (median: 4, IQR: 4–5; $P = .061$). Using the level of facial nerve bifurcation as the reference, although both radiologists were able to clearly distinguish the 2 main branches on both sequences, the IQS of the CISS for the temporofacial (median: 4, IQR: 4–4) and cervicofacial (median: 4, IQR: 4–4) division displays were significantly higher than those of the DESS-WE for the temporofacial (median: 3, IQR: 3–4) and cervicofacial (median: 3, IQR: 3–4) division displays ($P < .001$; Fig 3 and Online Supplemental Data).

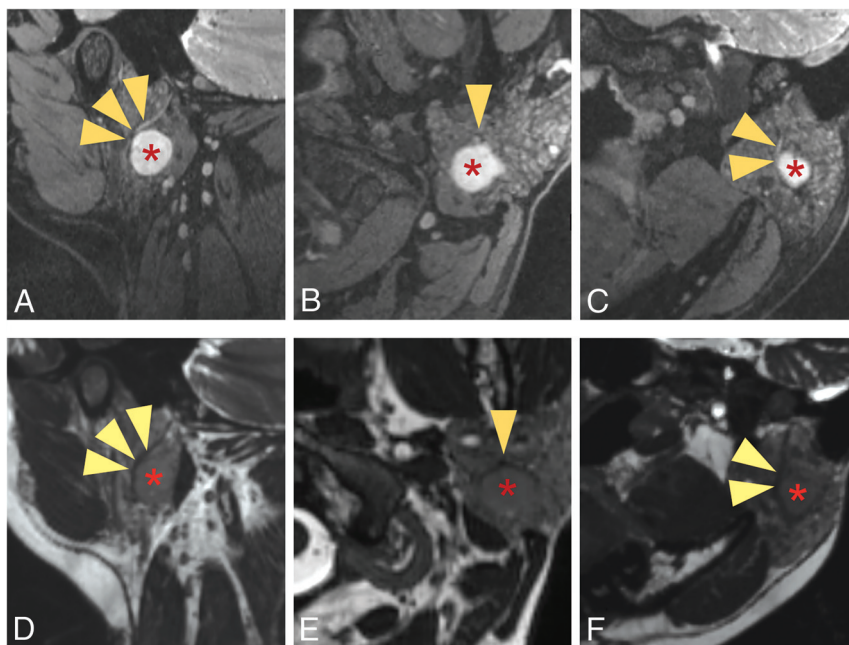


FIG 2. Image quality assessment of parotid tumors. Representative images of the clarity of tumor lesions in DESS-WE sequence (A–C) and CISS sequence (D–F); the continuity of the facial nerve to the level of the tumor in the oblique sagittal plane (A, D); and the relative position of the facial nerve to the tumor and the diagnostic confidence of the tumor localization in the oblique sagittal (A, D), transverse (B, E), and oblique coronal planes (C, F). Yellow arrowheads identify the main trunk of the facial nerve, and red asterisks (*) denote the tumor.

Table 2: SNR and CNR of DESS-WE and CISS

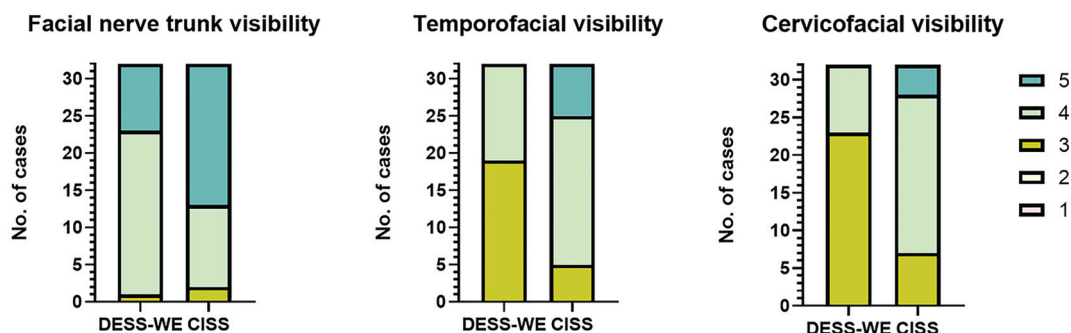
Participants		DESS-WE Mean \pm SD (Range)	CISS Mean \pm SD (Range)	<i>P</i>
SNR	Healthy volunteers	17.14 \pm 3.19 (9.42–21.99)	49.81 \pm 11.27 (29.65–73.27)	$<.001$
	Patients	17.13 \pm 5.00 (8.27–26.34)	46.85 \pm 14.11 (30.26–102.45)	$<.001$
	Overall	17.14 \pm 4.13 (8.27–26.34)	48.38 \pm 12.70 (29.65–102.45)	$<.001$
CNR	Healthy volunteers	7.07 \pm 2.39 (2.88–11.73)	54.10 \pm 17.07 (25.18–91.20)	$<.001$
	Patients	7.26 \pm 3.65 (1.49–14.83)	50.45 \pm 13.39 (29.39–80.24)	$<.001$
	Overall	7.21 \pm 2.94 (1.49–14.83)	52.33 \pm 15.38 (24.18–91.20)	$<.001$

Table 3: Intra- and interrater agreements for the image quality of DESS-WE and CISS

	Participants	Segmentation	DESS-WE	CISS
Interrater κ (95% CI)	Healthy volunteers	Facial nerve trunk visibility	0.724 (0.477–0.971)	0.796 (0.660–0.994)
		Temporofacial trunk visibility	0.753 (0.533–0.972)	0.816 (0.644–0.988)
		Cervicofacial trunk visibility	0.738 (0.522–0.954)	0.809 (0.635–0.983)
Intrarater κ (95% CI)	Healthy volunteers	Facial nerve trunk visibility	0.740 (0.503–0.977)	0.783 (0.580–0.995)
		Temporofacial trunk visibility	0.759 (0.553–0.966)	0.805 (0.623–0.986)
		Cervicofacial trunk visibility	0.728 (0.487–0.968)	0.755 (0.557–0.952)
Interrater κ (95% CI)	Patients	Clarity of tumor margin	0.841 (0.692–0.989)	0.797 (0.625–0.968)
		Continuity	0.810 (0.646–0.974)	0.774 (0.551–0.997)
		Spatial relationship	0.793 (0.624–0.963)	0.784 (0.575–0.993)
		Diagnostic confidence	0.784 (0.638–0.931)	0.780 (0.566–0.994)
Intrarater κ (95% CI)	Patients	Clarity of tumor margin	0.817 (0.651–0.982)	0.763 (0.584–0.943)
		Continuity	0.794 (0.604–0.982)	0.757 (0.568–0.946)
		Spatial relationship	0.854 (0.726–0.983)	0.779 (0.563–0.996)
		Diagnostic confidence	0.870 (0.750–0.989)	0.786 (0.584–0.989)

Note:—Continuity indicates continuity of the facial nerve trunk from the foramen to the level of the parotid tumor; spatial relationship, the relative position of the facial nerve in relation to the tumor.

Healthy volunteers



Patients with parotid tumors

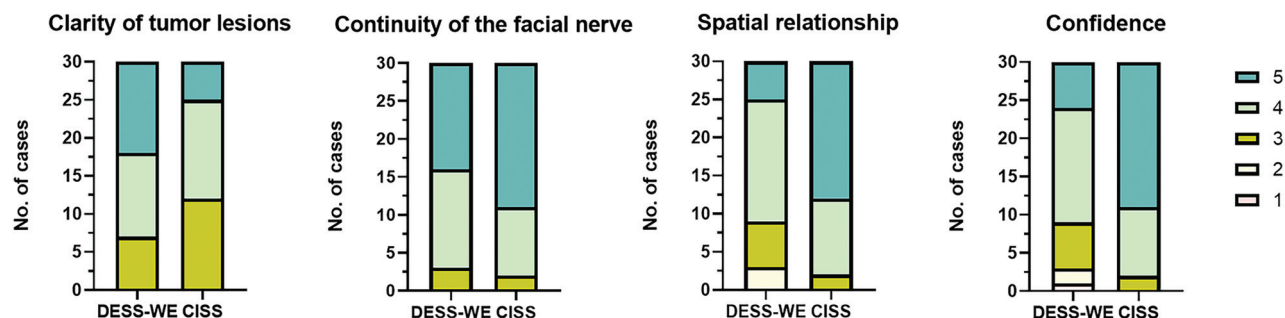


FIG 3. Subjective evaluation of the quality of DESS-WE and CISS images. All subgroups, including 16 healthy volunteers (32 facial nerves) and 25 patients (30 parotid tumors), were scored on a 5-point scale for multiple parameters, with scores of ≥ 3 indicating satisfactory quality and scores of 1–2 indicating unsatisfactory quality.

Subjective Evaluation of DESS-WE and CISS Images in Patients with Parotid Tumors

In patients with parotid tumors, subjective evaluation of the quality of the 2 sets of images by the 2 radiologists showed good agreement, with κ values >0.750 (Table 3). Although the score of the clarity of tumor margin was lower on CISS (median: 4, IQR: 3–4) than on DESS-WE images (median: 4, IQR: 3.75–4; $P = .018$), both techniques scored well in terms of the continuity of the main trunk of the facial nerve from the foramen to the level of

the parotid tumor, without statistically significant differences between DESS-WE (median: 4, IQR: 4–5) and CISS (median: 5, IQR: 4–5; $P = .083$). The scores in terms of visualizing the spatial relationships between tumors and facial nerves, and the level of diagnostic confidence, were both higher for CISS than for DESS (both $P < .001$; Fig 3 and Online Supplemental Data). However, in 3 patients, diagnostic confidence was scored as <3 owing to large tumor sizes that resulted in poor visualization of the spatial relationship between the tumor and facial nerve on DESS-WE images.

Table 4: Visibility of the DESS-WE and CISS images for the localization of parotid tumors (n = 30)

Imaging Findings	Surgical Findings		Diagnostic Performance			
	Deep Lobe +	Deep Lobe –	AUC (95% CI)	Accuracy	Sensitivity	Specificity
DESS-WE						
Deep lobe +	4	3	0.942 (0.792–0.994)	90%	100%	88.5%
Deep lobe –	0	23				
CISS						
Deep lobe +	4	1	0.981 (0.850–1.000)	96.7%	100%	96.2%
Deep lobe –	0	25				
P			0.1489			

Note:—AUC indicates area under the curve.

Evaluation of the Diagnostic Efficacy of Parotid Tumor Localization

Surgical findings confirmed that 26 lesions were localized to the superficial lobe, whereas 4 had components involving the deep lobe. The areas under the curve in terms of parotid tumor localization by using DESS-WE and CISS were 0.942 (95% CI, 0.792–0.994) and 0.981 (95% CI, 0.850–1.000), respectively. Both, therefore, represented excellent methods for the purpose; there was no significant difference between the two ($P = .1489$; Table 4).

DISCUSSION

The results of this study indicated that CISS had better performance in identifying intraparotid facial nerve branches compared with DESS-WE. Specifically, CISS can show the spatial relationship between the intraparotid facial nerve and parotid tumors with excellent agreement with intraoperative findings and can satisfy the requirements for preoperative surgical planning.

As has been shown previously, DESS-WE images are able to trace the facial nerve trunk and show a high level of accuracy (Kim et al,¹⁹ 92% versus Fujii et al,²¹ 97.8%) for localizing deep-lobe tumors in patients with parotid tumors—a finding that is consistent with our results. However, the overall accuracy of localizing deep-lobe tumors in this study was lower than what was reported in an earlier study by Fujii et al (97.8%),²¹ possibly because they included more deep-lobe lesions (25.2%). Although we had fewer deep-lobe tumors (13.3%), the proportion observed in our study is in line with the reported incidence of deep-lobe tumors in the parotid gland (10%).²⁹ We observed that CISS images were as effective for localizing parotid tumors as DESS-WE images, which is also consistent with the findings of Guenette et al (100%).²⁴ Although the CISS images scored lower in terms of the clarity of visualized tumors, CISS images scored higher in terms of the relative position of the facial nerve to the tumor. The relative position of the facial nerve to the tumor is the major concern from the surgeon's viewpoint because this can most affect the time needed for surgery, as well as postoperative facial function and aesthetics.^{11,30,31} The secondary branches of the intraparotid facial nerve (temporal, zygomatic, buccal, marginal mandibular, cervical) in patients with parotid tumors were not explored in this study, mainly because the surgeon's first step during parotid surgery is typically to identify the facial nerve trunk proximal to the tumor. Parotid tumors located superior to the main trunk of the facial nerve have a

significantly higher risk of facial nerve injury,³² and accurate identification of the main trunk of the facial nerve is a major factor in the attempt to avoid postoperative facial nerve injury.¹⁰ Therefore, observation of the trunk of the facial nerve is most important for surgical planning in most cases.

For 3 of our patients with parotid tumors, there was low diagnostic confidence in the DESS-WE sequences. This may be because in DESS-WE sequences, both the facial nerves and the tumors had high signal intensity.²⁶

Therefore, when the tumor was close to the facial nerve, there was less parotid parenchyma and little contrast distinction between them,²¹ making it difficult to determine the boundary between the two. This study also noted that the CNR of DESS-WE images was lower than that of CISS images, which is consistent with the findings of Hilgenfeld et al.³³ In patients with parotid tumors, CISS images were better than DESS-WE images in terms of visualizing the spatial relationship between the facial nerve and the tumor; therefore, even if the tumor is close to the facial nerve, the spatial relationship between the two can be clearly observed by using CISS.

We also observed that for normal parotid glands without tumors, DESS-WE sequences showed excellent performance regarding the facial nerve trunk. For the branches of the facial nerve (ie, the temporofacial and cervicofacial divisions), only limited assessments could be performed by using DESS-WE images¹⁹; however, CISS images with a high CNR showed more details of the facial nerve branches in the parotid gland and are more reliable for preoperative planning and enhancing clinician confidence in the surgical plans. These findings may have immediate implications for the performance of facial nerve MR imaging.

The DESS sequence involves the acquisition of 2 different echoes during each repetition time, formed from FISP and reversed fast imaging with steady state precession DWI sequence signals separately, which are then combined to form a single image.³⁴ The former provides more anatomic detail, whereas the latter accentuates the signal intensity with strong T2 contrast.³⁴ Meanwhile, combining the WE technique with the DESS sequence can clearly show the facial nerve itself without relying on the fatty tissue background.³⁵ In addition, the CISS sequence can differentiate between fat and parotid parenchyma, has high spatial resolution and high SNR, and is relatively insensitive to motion³⁴; this enables visualization of the extracranial facial nerve branches in the parotid gland, providing remarkable anatomical detail.³⁶ In this study, both DESS-WE and CISS images were able to identify the temporofacial and cervicofacial branches with good agreement, which is consistent with the findings ($\kappa > 0.70$) of Jeong et al.²²

This study has some limitations. First, this study included a small number of patients with deep-lobe tumors ($n = 4$), it did not have high statistical power, and it evaluated only the localization of the relationship between the main trunk of the facial

nerve and parotid lesions, with the clinical outcomes of the parotidectomy procedures not being compared between the patients. Second, only patients with first-time parotid tumors were included when we evaluated the visualization of the facial nerve, and patients with recurrence were not evaluated. As the surgical field is affected by scarring and fibrosis, identification of the facial nerve can become difficult. If the nerve can be identified during surgery for recurrent parotid tumors, the probability of successful preservation of the facial nerve is high.¹⁰ Lastly, this study only compared 2 sequences, CISS and DESS-WE, but reverse FISP and contrast-enhanced short-tau inversion recovery sequences also show good distinction of facial nerves; these were not simultaneously incorporated into the qualitative and quantitative analyses to determine the optimal protocol for examination of the extracranial segment of the facial nerve.

CONCLUSIONS

CISS achieved a diagnostic performance comparable with that of DESS-WE in terms of parotid tumor localization, with favorable image quality but more reliable morphologic visualization of the facial nerve. CISS images can provide surgeons with anatomic information regarding parotid tumors and facial nerves, alleviate the problem of facial nerve identification, and assist clinicians in planning optimal surgical approaches.

ACKNOWLEDGMENTS

We wish to thank our colleagues in the Radiology and Dental Departments who collaborated with us in the preparation of the manuscript, and we thank Mr. Yuanrui Li from MR Clinical Application of Siemens Healthineers and Ms. Chen Zhang from MR Research Collaboration of Siemens Healthineers for providing technical advice on CISS sequencing.

Disclosure forms provided by the authors are available with the full text and PDF of this article at www.ajnr.org.

REFERENCES

- Park W, Park J, Park SJ, et al. **Clinical outcomes and management of facial nerve in patients with parotid gland cancer and pretreatment facial weakness.** *Oral Oncol* 2019;89:144–49 [CrossRef Medline](#)
- Kawata R, Kinoshita I, Omura S, et al. **Risk factors of postoperative facial palsy for benign parotid tumors: outcome of 1,018 patients.** *Laryngoscope* 2021;131:E2857–E2864 [CrossRef Medline](#)
- Bittar RF, Ferraro HP, Ribas MH, et al. **Facial paralysis after superficial parotidectomy: analysis of possible predictors of this complication.** *Braz J Otorhinolaryngol* 2016;82:447–51 [CrossRef Medline](#)
- Olsen KD, Quer M, De Bree R, et al. **Deep lobe parotidectomy—why, when, and how?** *Eur Arch Otorhinolaryngol* 2017;274:4073–78 [CrossRef Medline](#)
- Saadya A, Chegini S, Morley S, et al. **Augmented reality presentation of the extracranial facial nerve: an innovation in parotid surgery.** *Br J Oral Maxillofac Surg* 2023;61:428–36 [CrossRef Medline](#)
- Ruohoaho J, Makitie AA, Aro K, et al. **Complications after surgery for benign parotid gland neoplasms: a prospective cohort study.** *Head Neck* 2017;39:170–76 [CrossRef Medline](#)
- Hohman MH, Bhama PK, Hadlock TA. **Epidemiology of iatrogenic facial nerve injury: a decade of experience.** *Laryngoscope* 2014;124:260–65 [CrossRef Medline](#)
- Jin H, Kim BY, Kim H, et al. **Incidence of postoperative facial weakness in parotid tumor surgery: a tumor subsite analysis of 794 parotidectomies.** *BMC Surg* 2019;19:199 [CrossRef Medline](#)
- Sood AJ, Houlton JJ, Nguyen SA, et al. **Facial nerve monitoring during parotidectomy: a systematic review and meta-analysis.** *Otolaryngol Head Neck Surg* 2015;152:631–37 [CrossRef Medline](#)
- Kuriyama T, Kawata R, Higashino M, et al. **Recurrent benign pleomorphic adenoma of the parotid gland: facial nerve identification and risk factors for facial nerve paralysis at re-operation.** *Auris Nasus Larynx* 2019;46:779–84 [CrossRef Medline](#)
- Kinoshita I, Kawata R, Higashino M, et al. **Tumor localization is the important factor for recovery time of postoperative facial nerve paralysis in benign parotid surgery.** *Auris Nasus Larynx* 2023;51:214–20 [CrossRef Medline](#)
- Aasen MH, Hutz MJ, Yuhun BT, et al. **Deep lobe parotid tumors: a systematic review and meta-analysis.** *Otolaryngol Head Neck Surg* 2022;166:60–67 [CrossRef Medline](#)
- Zenga J, Lin BM, Chen J, et al. **Microsurgical instrument-assisted facial nerve dissection for deep lobe parotid tumors.** *Laryngoscope* 2018;128:2529–31 [CrossRef Medline](#)
- Attie A, Karkas A, Tropres I, et al. **Parotid gland tumours: MR tractography to assess contact with the facial nerve.** *Eur Radiology* 2016;26:2233–41 [CrossRef Medline](#)
- Castellaro M, Moretto M, Baro V, et al. **Multishell diffusion MRI-based tractography of the facial nerve in vestibular schwannoma.** *AJNR Am J Neuroradiol* 2020;41:1480–86 [CrossRef Medline](#)
- Rouchy RC, Attie A, Medici M, et al. **Facial nerve tractography: a new tool for the detection of perineural spread in parotid cancers.** *Eur Radiology* 2018;28:3861–71 [CrossRef Medline](#)
- Hussain T, Nguyen LT, Whitney M, et al. **Improved facial nerve identification during parotidectomy with fluorescently labeled peptide.** *Laryngoscope* 2016;126:2711–17 [CrossRef Medline](#)
- Chu J, Zhou Z, Hong G, et al. **High-resolution MRI of the intraparotid facial nerve based on a microsurface coil and a 3D reversed fast imaging with steady-state precession DWI sequence at 3T.** *AJNR Am J Neuroradiol* 2013;34:1643–48 [CrossRef Medline](#)
- Kim Y, Jeong HS, Kim HJ, et al. **Three-dimensional double-echo steady-state with water excitation magnetic resonance imaging to localize the intraparotid facial nerve in patients with deep-seated parotid tumors.** *Neuroradiology* 2021;63:731–39 [CrossRef Medline](#)
- Zhao Y, Yang B. **Value of visualization of the intraparotid facial nerve and parotid duct using a micro surface coil and three-dimensional reversed fast imaging with steady-state precession and diffusion-weighted imaging sequence.** *J Craniofac Surg* 2018;29:e754–e57 [CrossRef Medline](#)
- Fujii H, Fujita A, Kanazawa H, et al. **Localization of parotid gland tumors in relation to the intraparotid facial nerve on 3D double-echo steady-state with water excitation sequence.** *AJNR Am J Neuroradiol* 2019;40:1037–42 [CrossRef Medline](#)
- Jeong HS, Kim Y, Kim HJ, et al. **Imaging of facial nerve with 3D-DESS-WE-MRI before parotidectomy: impact on surgical outcomes.** *Korean J Radiology* 2023;24:860–70 [CrossRef Medline](#)
- Ozdemir M, Kavak RP. **Morphometric analysis of facial and cochlear nerves in normal-hearing ears using 3D-CISS.** *J Otol* 2019;14:136–40 [CrossRef Medline](#)
- Guenette JP, Ben-Shlomo N, Jayender J, et al. **MR imaging of the extracranial facial nerve with the CISS sequence.** *AJNR Am J Neuroradiol* 2019;40:1954–59 [CrossRef Medline](#)
- Guenette JP, Seethamraju RT, Jayender J, et al. **MR imaging of the facial nerve through the temporal bone at 3T with a noncontrast ultra-short echo time sequence.** *AJNR Am J Neuroradiol* 2018;39:1903–06 [CrossRef Medline](#)
- Qin Y, Zhang J, Li P, et al. **3D double-echo steady-state with water excitation MR imaging of the intraparotid facial nerve at 1.5T: a pilot study.** *AJNR Am J Neuroradiol* 2011;32:1167–72 [CrossRef Medline](#)
- Landis JR, Koch GG. **The measurement of observer agreement for categorical data.** *Biometrics* 1977;33:159–74 [CrossRef](#)

28. Benchoufi M, Matzner-Lober E, Molinari N, et al. **Interobserver agreement issues in radiology.** *Diagn Interv Imaging* 2020;101:639–41 [CrossRef Medline](#)
29. Harney MS, Murphy C, Hone S, et al. **A histological comparison of deep and superficial lobe pleomorphic adenomas of the parotid gland.** *Head Neck* 2003;25:649–53 [CrossRef Medline](#)
30. Kim JK, Lee DW, Geum S, et al. **Ultrasonographic localization of parotid gland tumor relative to the facial nerve using Stensen's duct criterion.** *J Oral Maxillofac Surg* 2023;81:1055–61 [CrossRef Medline](#)
31. El Kininy W, Roddy D, Davy S, et al. **Magnetic resonance diffusion weighted imaging using constrained spherical deconvolution-based tractography of the extracranial course of the facial nerve.** *Oral Surg Oral Med Oral Pathol Oral Radiology* 2020;130:e44–e56 [CrossRef Medline](#)
32. Chiesa-Estomba CM, Echaniz O, Sistiaga Suarez JA, et al. **Machine learning models for predicting facial nerve palsy in parotid gland surgery for benign tumors.** *J Surg Res* 2021;262:57–64 [CrossRef Medline](#)
33. Hilgenfeld T, Saleem MA, Schwindling FS, et al. **High-resolution single tooth MRI with an inductively coupled intraoral coil-can MRI compete with CBCT?** *Invest Radiology* 2022;57:720–27 [CrossRef Medline](#)
34. Chavhan GB, Babyn PS, Jankharia BG, et al. **Steady-state MR imaging sequences: physics, classification, and clinical applications.** *Radiographics* 2008;28:1147–60 [CrossRef Medline](#)
35. Eckstein F, Hudelmaier M, Wirth W, et al. **Double echo steady state magnetic resonance imaging of knee articular cartilage at 3 Tesla: a pilot study for the Osteoarthritis Initiative.** *Ann Rheum Dis* 2006;65:433–41 [CrossRef Medline](#)
36. Wen J, Desai NS, Jeffery D, et al. **High-resolution isotropic three-dimensional MR imaging of the extraforaminal segments of the cranial nerves.** *Magn Reson Imaging Clin N Am* 2018;26:101–19 [CrossRef Medline](#)